

Molecular modeling, structure activity relationship and immunomodulatory properties of some lupeol derivatives

Mohsen Shahlaei · Syed Mustafa Ghanadian · Abdul Majid Ayatollahi · M. Ahmed Mesaik · Omer Mohamed Abdalla · Suleiman Afsharypour · Mohammed Rabbani

Received: 2 April 2012 / Accepted: 25 July 2012 / Published online: 5 August 2012
© Springer Science+Business Media, LLC 2012

Abstract Currently, scientists are focused on developing drug-like compounds as an alternative to the available immunosuppressive drugs with less side effects. Therefore, in the current study we tried to generate derivatives of lupeol and investigate their primary effects on the immune system. In the second part, a computational approach, integrating molecular docking, and molecular dynamics simulation was used to assess the likely mechanism of action and the preliminary analysis of the structure activity relationship (SAR). Our goal for this research was to develop an in-depth SAR for the design of future immunosuppressive lupeol analogs with the potential clinical use.

Keywords Drug design · Biologic screening · Natural product · Molecular modeling · Structure activity relationship

Introduction

Currently, triterpenes are being investigated in the treatment of autoimmune and non-autoimmune inflammatory diseases like allergic asthma (Ayatollahi *et al.*, 2011). In such diseases, neutrophils, as a source of inflammatory eicosanoids, cytokines, and tissue-degrading lysosomal enzymes, appear shortly after an irritating or noxious stimulus. Activation of primed neutrophils, either by phagocytosis of opsonized bacteria or by frustrated phagocytosis, generates the rapid production of ROS via the action of NADPH oxidase. Oxygen radicals cause oxidative damages to DNA, lipids, proteins, lipoproteins, and may be implicated in mutations to immunoglobulins leading toward the formation of rheumatoid factor (Helen *et al.*, 2010.). In such reactions, an increased level of cAMP has a suppressive effect on the oxidative burst in neutrophils (Bani *et al.*, 2006) where it is reported that cAMP-dependent PKA phosphorylates a protein (RAP 1a) belonging to the Ras superfamily which, in turn, blocks assembly of NADPH oxidase components into the active enzymatic complex (Ottonello *et al.*, 1995). Similarly, in peripheral blood lymphocytes, allergen-induced synthesis of IL-2, IL-4, and IL-5 is inhibited by cAMP elevating factors (Yeadon and Diamant, 2000). In this study, we tried to investigate the phagocytic oxidative burst and the lymphocyte proliferation properties of some Lupeol derivatives as well as their intermolecular interactions with adenyl cyclase (AC) (Fig. 1) to introduce new anti-inflammatory

M. Shahlaei
Department of Medicinal Chemistry, Faculty of Pharmacy,
Kermanshah University of Medical Sciences, Kermanshah,
Islamic Republic of Iran

S. M. Ghanadian (✉)
Isfahan Pharmaceutical Sciences Research Center,
Isfahan University of Medical Sciences, Isfahan,
Islamic Republic of Iran
e-mail: phytochemistry.center@gmail.com;
ghanadian@pharm.mui.ac.ir

A. M. Ayatollahi
Phytochemistry Research Center, Shahid Beheshti University
of Medical Sciences, Tehran, Islamic Republic of Iran

M. A. Mesaik · O. M. Abdalla
Dr. Panjwani Center for Molecular Medicine and Drug Research,
International Center for Chemical and Biological Sciences,
University of Karachi, Karachi 75270, Pakistan

S. Afsharypour · M. Rabbani
Faculty of Pharmacy and Pharmaceutical Sciences,
Isfahan University of Medical Sciences, Isfahan,
Islamic Republic of Iran

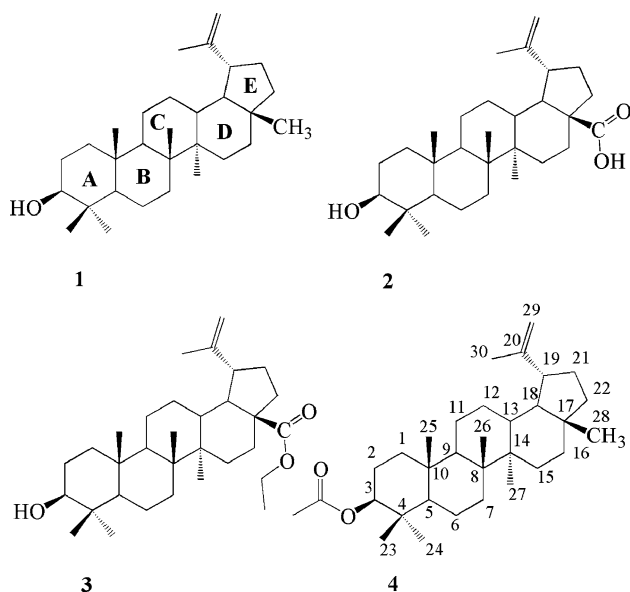


Fig. 1 Chemical structures of lupeol (**1**), betulinic acid (**2**), ethyl betulinate (**3**), and lupenyl acetate (**4**)

and immunosuppressive agents. Recently, pentacyclic triterpenes have been widely reported to exhibit anti-inflammatory activities (Yogeeswari and Sriram, 2005; Einzhammer and Xu, 2004). Based on these studies, changes in the size of ring E, or the nucleophilicity, and the strength of hydrogen bonding capability or acidity at C-19, C-20, and C-28 positions are responsible for their differences in biologic effects. Therefore, making derivatives by modification in these positions are assumed to improve their immunomodulatory activities.

Materials and methods

Extraction and isolation of lupane-type triterpenes

Aerial flowering parts of *Euphorbia aellenii* Rech. F. (Euphorbiaceae) were collected in August 2007 from Northern Khorasan province (Iran) and a voucher specimen (no. 2024) of the plant has been deposited in the herbarium of the Pharmacognosy Department, School of Pharmacy and Pharmaceutical sciences at the Isfahan University of Medical Sciences (Iran). Air-dried plant was ground to fine powder (7 kg) and macerated for 4 days with MeOH (20 L × 3) at room temperature. Filtration and in vacuo evaporation resulted in a green gum (500 g) which was partitioned between methanol and *n*-hexane. The defatted extract was concentrated, dissolved in water, and successively extracted with chloroform, ethyl acetate, and *n*-butanol. The chloroform fraction (240 g) was subjected to column chromatography over the normal silica gel using hexane/chloroform mixtures of increasing polarity up to

100 %. Hexane/chloroform (20:80) fraction was further purified using gradient mixtures of hexane/ethyl acetate (0 → 50) on silica to afford several fractions. Inferred by ¹H-NMR spectra, Fr.2 and Fr.5 fractions containing triterpenes were further purified on Sephadex (dichloromethane/methanol, 1:2) to yield subfraction rich in triterpenes, visible as violet spots on thin layer chromatography (TLC). Finally, Fr.2a and Fr.5a were subjected to recycle HPLC Jaigel-2H&1H columns with chloroform as mobile phase to obtain compounds **1**, and **2** identified by comparing their NMR, Mass, and spectroscopic data with those reported in the literature (Macias *et al.*, 1994; Domínguez-Carmona *et al.*, 2010; Viqar and Rahman, 1994).

Synthesis of derivatives

Ethyl betulinate (3). A mixture of betulinic acid (13.5 mg), K₂CO₃ (200 mg), C₂H₅I (1 mL), and acetone (1 mL) was stirred for 72 h at room temperature. When reached to the end point, the reaction mixture was poured over distilled water (13 mL) and extracted twice with ethyl acetate (4:1). The organic layer was dried with anhydrous Na₂SO₄, filtered, and the solvent was evaporated to obtain esterified product. Then, the esterified compound was purified more through preparative layer chromatography (hexane: ethyl acetate, 7:3) and confirmed by H-NMR and mass spectra (Domínguez-Carmona *et al.*, 2010).

Lupenyl acetate (4). 10 mg, separately with acetic anhydride (1 mL) and pyridine (0.5 mL), were stirred at room temperature for 3 days. At the final point of reaction, the mixture was poured over ice and extracted twice with ethyl acetate (2:1 v/v). The organic phase was washed with equal volumes of HCl (5 %), NaOH (3 %), H₂O, and NaCl saturated followed by drying over anhydrous Na₂SO₄. After filtration, the solvent evaporated in vacuo to yield the acetylated product which was then confirmed through H-NMR and Mass spectra (Domínguez-Carmona *et al.*, 2010).

Lupeol (1)

White powder, mp 215–217; IR (KBr) λ max: 3440, 1648, 1605, 1280, 1025, 880 cm⁻¹; ¹H-NMR (CDCl₃, 300 MHz) δ _H, mult., *J* in Hz 4.67, 4.55 (each 1H, dd, *J* = 2.4, 1.5, H-29), 3.17 (1H, dd, *J* = 10.8, 5.2, H-3), 2.36 (1H, dt, *J* = 10.7, 6.0, H-19), 1.71 (3H, s, H-30), 1.01, 0.96, 0.92 (each 3H, s, H-2, 27, 23), 0.81, 0.77, 0.74 (each 3H, s, H-25, 28, 24); ¹³C-NMR (CDCl₃, 100 MHz) δ _C 38.69 (C-1), 27.4 (C-2), 78.9 (C-3), 38.9 (C-4), 55.3 (C-5), 18.3 (C-6), 34.2 (C-7), 40.8 (C-8), 50.4 (C-9), 37.2 (C-10), 20.9 (C-11), 25.1 (C-12), 38.0 (C-13), 42.8 (C-14), 27.4 (C-15), 35.5 (C-16), 43.0 (C-17), 48.3 (C-18), 48.0 (C-19), 151.0 (C-20), 29.8 (C-21), 40.0 (C-22), 27.9 (C-23), 16.0 (C-24),

18.0 (C-25), 16.1 (C-26), 14.6 (C-27), 15.4 (C-28), 109.3 (C-29), 19.3 (C-30); EI-HRMS of m/z 426.6998 (calc. for $C_{30}H_{50}O$, 426.7194); EI-MS m/z 426, 424, 411, 316, 315, 257, 234, 229, 218, 205, 203, 189, 175, 149, 147, 133, 123, 121, 119, 105, 95, 55.

Betulinic acid (2)

Needle crystals, mp 294–296; IR (KBr) λ max: 3446, 2924, 2862, 1685, 1645 1604, 1236, 1107, 1034; 1H -NMR ($CDCl_3$, 300 MHz) δ_H , mult., J in Hz: 4.72, 4.59 (each 1H, br-s, H-29), 3.17 (1H, dd, $J = 5.1, 10.8$ Hz, H-3), 2.98 (1H, dt, $J = 11.1, 3.0$, H-19), 1.67 (3H, s, H-30), 0.95, 0.94, 0.91 (each 3H,s, H-26, 27, 23), 0.80, 0.73 (each 3H, s, H-25, 24); ^{13}C -NMR ($CDCl_3$, 100 MHz) δ_c : 38.6 (C-1), 27.0 (C-2), 78.8 (C-3), 38.7 (C-4), 55.3 (C-5), 18.2 (C-6), 34.2 (C-7), 40.6 (C-8), 50.4 (C-9), 37.0 (C-10), 20.8 (C-11), 25.4 (C-12), 38.2 (C-13), 42.3 (C-14), 30.5 (C-15), 32.1 (C-16), 56.1 (C-17), 49.1 (C-18), 46.9 (C-19), 150.6 (C-20), 37.0 (C-21), 29.6 (C-22), 27.5 (C-23), 15.2 (C-24), 15.8 (C-25), 16.0 (C-26), 14.5 (C-27), 179.1 (C-28), 19.2 (C-30), 109.4 (C-29). EI-HRMS of m/z 456.3606 (calc. for $C_{30}H_{48}O_3$, 456.3603); EI-MS m/z 456, 438, 423, 411, 395, 369, 356, 302, 248, 220, 207, 203, 189, 175, 135, 95, 69, 55.

Ethyl betulinate (3)

1H -NMR ($CDCl_3$, 500 MHz) δ_H , mult., J in Hz: 4.71 (1H, br-s, H-29a), 4.61 (1H, br-s, H-29b), 4.15 and 4.08 (each 1H, m, 28-COO-Et-H-1'a & H-1'b), 3.15 (1H, dd, $J = 5.0, 11.5$ Hz, H-3), 2.98 (1H, m, H-19), 1.66 (3H, s, H-30), 1.23 (3H, m, 28-COO-Et-H-2'), 0.94 (6H, br-s, H-26, 23), 0.89 (3H, s, H-27), 0.79 (3H, s, H-25), 0.73 (3H, s, H-24); CI-MS m/z 485 (M + 1), 467, 409, 393, 275, 206.

Lupenyl acetate (4)

1H -NMR ($CDCl_3$, 300 MHz) δ_H , mult., J in Hz 4.67, 4.56 (each 1 H, br-d, $J = 2.5$ Hz, H-29), 3.17 (dd, $J = 11.0, 5.2$, H-3), 2.04 (3H, s, $COCH_3$), 1.71, 1.00, 0.96 (each 3H, s, H-30, 26, 23), 0.92 (3H, s, H-27), 0.81, 0.77, 0.74 (each 3H, s, H-25, 28, 24); EI-MS m/z 468, 453, 357, 297, 276, 249, 218, 203, 189, 69, 55.

Biologic assays

Phagocyte chemiluminescence assay

As a parameter for evaluating phagocytosis in stimulated polymorphonuclear cells, formation of the reactive oxidants in whole blood was measured by the Luminol-enhanced chemiluminescence assay procedure (Mischak *et al.*, 1993). In brief, three concentrations of each

compound (0.5, 5, and 50 $\mu g/mL$) were prepared in 25 μL of Hank's Buffered Salt Solution containing calcium chloride and magnesium sulfate (HBSS⁺⁺) in 96-well flat-bottomed plates for a final incubation volume of 100 μL . Then, 25 μL of whole blood diluted 1:50 in suspension of HBSS⁺⁺ was added. Positive, negative, and blank control wells were included in the assay. Whole blood phagocytes and compounds were incubated for 30 min at 37 °C, then 25 μL luminol (Research Organics, Cleveland, OH, USA) was added into each well, and 25 μL serum opsonized zymosan (Fluka, Buchs, Switzerland) was finally added except for negative and blank wells. Kinetic production of the reactive oxygen species was monitored using the luminometer (Labsystems luminoskan, Helsinki, Finland) for 50 min in the repeated scan mode. Peak and total integral chemiluminescence reading were expressed as relative light unit (RLU).

Lymphocyte proliferation assay

Peripheral human blood lymphocytes were incubated with different concentrations of the test compounds (0.5, 5, and 50 $\mu g/mL$ in duplicates) in supplemented (10 % Fetal Bovine Serum) RPMI-1640 along with 5.0 $\mu g/mL$ phytohemagglutinin (Sigma Aldrich incorporation, USA) at 37 °C in CO_2 environment for 72 h. Further incubation for 18 h after the addition of 0.5 $\mu Ci/well$ 3H -thymidine (Amersham, Buckinghamshire, UK) was done and cells were harvested using the cell harvester (Inotech Dottikon, Switzerland). Finally, the proliferation level was determined by the radioactivity level as count per minute (CPM) recorded from the β -scintillation counter (Beckman coulter, LS 6500, Fullerton, CA, USA) (Nielsen *et al.*, 1998).

Molecular docking

Using the crystal structure, AC5 protein retrieved from the Protein Data Bank (PDB code: 1CJV), lupeol derivatives (1–3) were selected for docking process to study the molecular interactions between compounds of interest and their site of action. The optimized structures by a semi empirical method (AM1), implemented in HyperChem, were used as input of Auto Dock Tools and the partial charges of atoms were calculated by Gasteiger–Marsili procedure (1980). After determining Kollman united atom charges (Weiner *et al.*, 1984), non-polar hydrogens were merged to their corresponding carbons. As a final processing step in protein preparation, desolvation parameters were assigned to each atom. By means of auto grid tools, the grid maps were generated adequately large to include the active site of protein, as well as significant regions of the surrounding surface. In all cases, a grid map of 60 grid points and a grid spacing of 0.375 Å were applied in each

Cartesian direction. Considering the original ligand location in the complex, the maps were centered on the ligand's binding site, searching favorable interactions with the functional groups. Based on Lamarckian Genetic Algorithm (Morris *et al.*, 1998), by means of the pseudo-Solis and Wets local search method (Solis and Wets, 1981), Auto Dock Tools were employed to produce both grid and docking parameter files. Applying 2.0 Å clustering tolerance to construct clusters of the closest compounds, the initial coordinates of the ligand were used as the reference structure. Finally, docking results were investigated by VMD1.8.6 (Humphrey *et al.*, 1996).

Molecular dynamics simulation

Molecular dynamics (MD) simulation was carried out by means of GROMOS96 force-field through the GROMACS software (Ver. 4.5, www.gromacs.org). The structure of adenylyl cyclase 5 and ethyl betulinate ligand, as a representative, obtained from the docking procedure were used as a starting point for the MD simulation. Protein and ligand were soaked in a cubic box of SPC (Single Point Charge) water molecules (Berendsen *et al.*, 1981) and simulated using periodic boundary conditions. All the protein atoms were at a distance equal or greater than 0.7 nm from the box edges. MD simulation was carried in the isobaric-isothermal ensemble (NPT: 300 K and 1 bar). By means of the productive MD, pressure was kept constant at 1 bar by altering the box dimensions and the time constant for pressure coupling was set to 1 ps. The LINCS (Hess *et al.*, 1997) algorithm was employed to constrain bond lengths, permitting the application of 2 fs time step. The Particle Mesh Ewald method (PME) was used in the computation of the electrostatic forces (Darden *et al.*, 1993). Van der Waals and Coulomb interactions were calculated within a cutoff of 10 Å.

Statistical analysis

The IC_{50} values were calculated by means of a Excel-based program and reported as mean \pm SD of the mean. Significance was attributed to p -values ($p < 0.05$), and the probability values were obtained by the Student t test between sample and control data.

Results and discussion

Chemistry

Compound **1** was identified as $C_{30}H_{50}O$ (calculated: 426.7194) based on positive EI-HRMS of m/z 426.6998. Six degrees of unsaturation, ^{13}C -NMR, and DEPT spectral

data supported one double bond and therefore, five rings in the molecule. Seven singlet methyls at δ_H 1.71, 1.01, 0.96, 0.92, 0.81, 0.77, and 0.74, along with a pair of olefinic protons as a part of an exocyclic-methylene group at δ_H 4.67 and 4.55 together with a doublet of triplet of one proton at δ_H 2.36 ($J = 10.7, 6$ Hz) characteristic for lupane triterpenes (Ayatollahi *et al.*, 2011) were observed in the 1H -NMR spectrum. The existence of one hydroxyl group was also evident by NMR signals at δ_H 3.17. Taken together, the spectral data of **1** was in complete accordance with those previously reported for Lupeol (Viqar and Rahman, 1994). Compound **2** was also identified as betulinic acid based on its similarities with compound **1** except for additional acidic carbonyl group at δ_c 179.1 instead of C-28 singlet methyl at δ_c 15.4 (Viqar and Rahman, 1994). The structures of derivatives were also confirmed by comparing their 1H -NMR and mass data with those reported in the literature (Domínguez-Carmona *et al.*, 2010; Viqar and Rahman, 1994).

Biologic assays

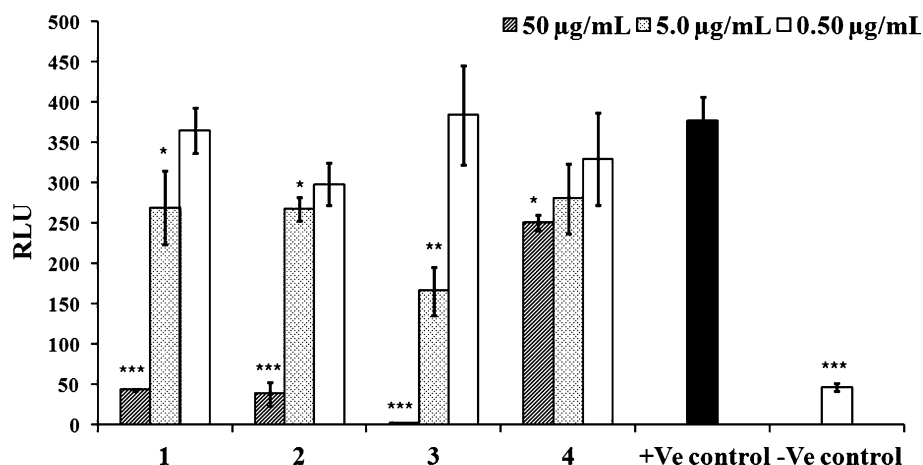
Phagocyte chemiluminescence

Phagocytic cells, on activation, produce reactive oxygen-free radicals which are then quantified by a luminol-enhanced chemiluminescence assay. A comparison of the phagocytic oxidative burst activity in the presence of varying concentrations (0.5–50 $\mu g/mL$) of compounds (**1–4**) is shown in Fig. 2. Lupeol (**1**) and betulinic acid (**2**) showed a dose-dependent decrease in the oxidative burst in neutrophils with IC_{50} : 11.35 ± 3.47 , and 11.12 ± 1.77 , respectively. Phagocyte chemiluminescence decreased significantly (41.12 ± 2.32 % at 50 $\mu g/mL$) by masking the free 3-OH group in lupenyl acetate (**4**) and substitution of C-28 hydrophilic acidic group in betulinic acid with esteric group in ethyl betulinate (**3**) showed further suppressive activity with IC_{50} value of 3.85 ± 1.30 $\mu g/mL$.

T cell proliferation assay

The anti-proliferation effect of the test compounds was determined by measuring the PHA-induced T cell proliferation by determining radioactive thymidine incorporation. Lupeol (**1**) showed a dose-dependent decrease in lymphocyte proliferation with IC_{50} of 13.16 ± 0.9 $\mu g/mL$ in conformity with another study by Bani *et al.* (2006) which showed suppressive action against cytotoxic CD8+ and helper CD4+ T cells in balb/c mice. In comparison, lupenyl acetate (**4**), with masked 3-OH group, showed a significantly decreased inhibitory effect (38.92 ± 9.39 % at 50 $\mu g/mL$), while ethyl betulinate (**3**), with esteric amphoteric group at C-28, presented an improved

Fig. 2 Effect of compounds 1–4 on the neutrophils oxidative burst. The luminol-dependent chemiluminescence induced by zymosan in the presence of lupeol (1), betulinic acid (2), ethyl betulinic acid (3), and lupenyl acetate (4) compared to the controls (+ve, -ve). Data were presented as mean \pm SD for three measurements. One-way ANOVA was used to calculate p value against the positive control (* p < 0.05, ** p < 0.01, and *** p < 0.001). RLU relative light units



inhibitory effect with IC_{50} value of 12.9 ± 0.8 $\mu\text{g/mL}$. Addition of betulinic acid (2) in the concentration ranges 0.5, 5 and 50 $\mu\text{g/mL}$ resulted in stimulation of lymphocyte proliferation at 50 $\mu\text{g/mL}$ by 38.2 ± 2.78 % agreed with another report on increasing cellular and humoral immunity by betulinic acid that stimulated the proliferation of mice thymocytes, splenocytes, and human PBMC in a time and dose-dependent manner (Yi *et al.*, 2010).

Molecular docking

Through adenylyl cyclase (AC) pathway, cyclic AMP-elevating agents downregulate the oxidative burst induced by neutrophils (Bani *et al.*, 2006). The activation of adenylyl cyclase converts adenosine triphosphate (ATP) into cyclic adenosine monophosphate (cAMP) which starts a negative signal pathway that reduces T cell activation process (Bani *et al.*, 2006) and cytokine production (Aandahl *et al.*, 2002). Among different known types of AC in mammals, type 5 adenylyl cyclase (AC5) is known to be widely distributed in the body with multiple regulatory functions including immunomodulatory action (Ruppelt *et al.*, 2007). Clarification of ligand binding mechanisms is one of the essential steps to introduce more selective and potent lead compounds for a given target protein. To facilitate this, computational methods, such as docking and MD simulation, are among the best approaches for the estimation of protein–ligand interactions. First, for the validation of selected parameters and condition of docking procedure, an internal validation phase was carried out. In this step of docking, 5'-Guanosine-diphosphate-monothiooosphate was docked onto AC5 (the lowest energy pose for docking is shown in Fig. 3). Superimposing the experimental and predicted conformations, the RMSD was achieved as 1.16 Å which considered as a successfully docked (Erickson *et al.*, 2004). After internal validation phase, docking process was performed on AC5 binding pocket using tested compounds (1–4). The 200 docking

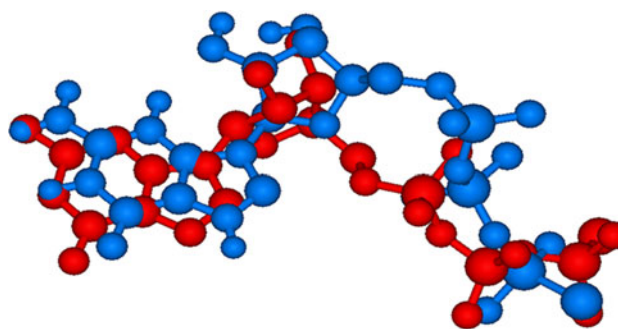


Fig. 3 Internal validation phase result; conformational overlaid of 5'-guanosine-diphosphate-monothiooosphate retrieved from crystal structure (red structure) with that from Auto Dock model (blue structure)

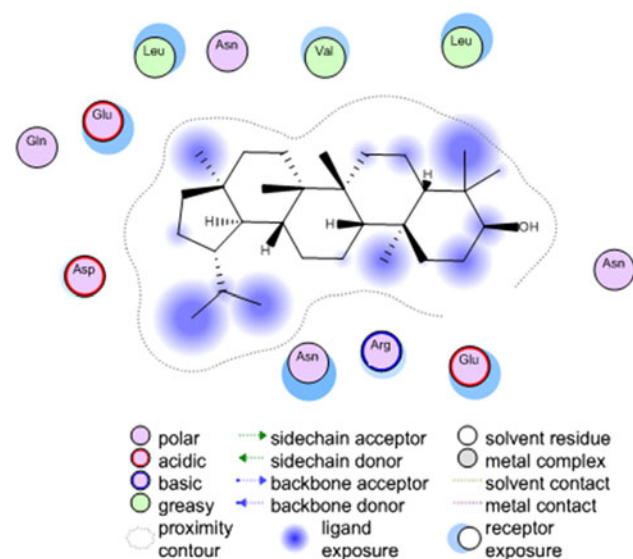
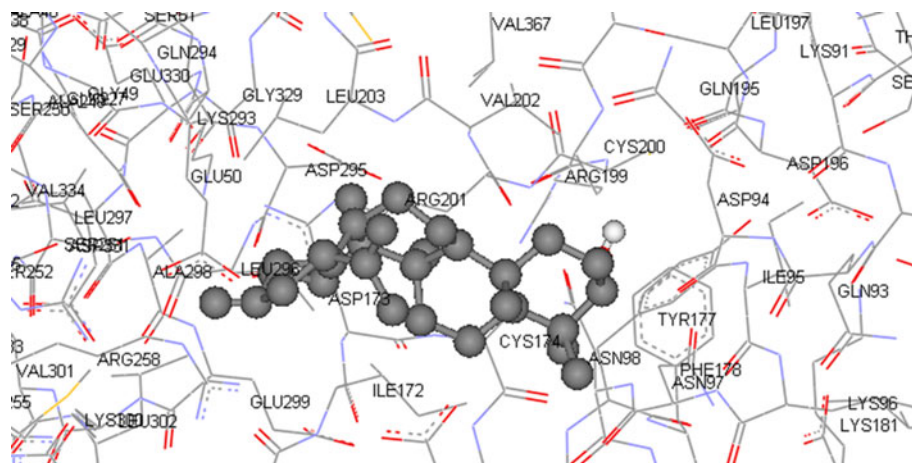
geometries for each investigated ligand were separated into clusters according to RMSD tolerance criterion. Besides RMSD cluster analysis, Auto Dock also applies binding-free energy assessment to assign the best binding conformation. Energy items estimated by Auto Dock are described by intermolecular energy (including van der Waals energy, hydrogen bonding energy, desolvation energy, and electrostatic energy), internal energy, and torsional free energy (Table 1). In addition, with respect to the docking results, the procedure successfully placed the ligands into a binding cavity among the Asn98, Leu298, Ala298, and Glu50 (Figs. 4, 5).

Molecular dynamics simulation and structure activity relationship

As discussed above, we initially applied simple docking of the ligand into the AC5 binding pocket. These results were not conclusive because binding of ligand to a protein is a dynamic process, and molecular docking alone can only stand for instantaneous states and cannot provide complete information on the best stable binding modes of ligand to the receptor (Shahlaei *et al.*, 2010a, b). Therefore,

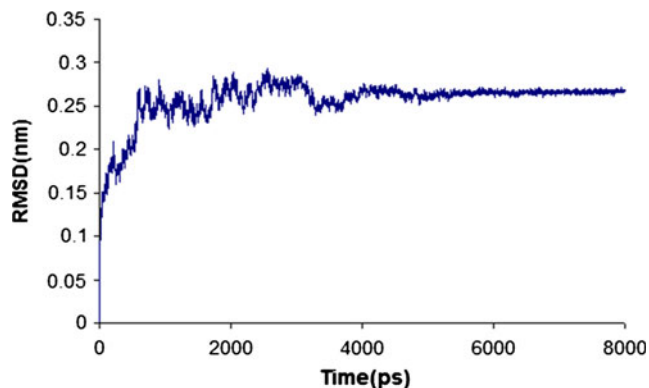
Table 1 Values of various energies (in Kcal/mol) resulted from docking process for compound 1–4

Compound	Final intermolecular energy	vdW + Hbond + desolv energy	Electrostatic energy	Internal energy	Torsional free energy	Binding energy	Docking energy
1	-5.78	-5.77	-0.01	-0.46	2.98	-2.8	-6.24
2	-4.84	-5.23	0.38	-0.37	2.98	-1.86	-5.21
3	-5.85	-6.00	0.15	-0.68	2.98	-2.87	-6.53
4	-6.18	-6.02	-0.16	-0.53	2.98	-3.2	-6.71

Fig. 4 Docking simulation result of ethyl betulinate**Fig. 5** 2D scheme of interactions between ethyl betulinate and active site

molecular dynamics simulation was carried out on the most effective compound, ethyl betulinate (compound 3) to gain further insight into the mechanism (s) that could explain the experimentally observed activity and to cross check our findings from docking. Worthy of attention, that what we can expect from molecular dynamics simulations of

protein (s), is that such MD simulations give complete details of the motions of protein and ligand (s) in the system so the thermodynamic properties could be estimated. Figure 6 shows the root mean-square deviation (RMSD) of the C_{α} atoms of protein in the simulation with respect to AC5 in the crystal structure. Within the first 2 ns of MD, the RMSD with respect to the initial structure rapidly increases to a value near 2.7 Å. After fluctuating around this value for a further 2 ns, the RMSD was not increased significantly. The RMSD value implies that this protein structure has been affected by its docked ligand and environment dramatically.

**Fig. 6** C_{α} RMSD of adenylyl cyclase 5 during the molecular dynamic simulation

It can be seen that the protein–ligand complex immersed among water molecules stays in equilibrium throughout the MD. Then, we deduce that the MD simulation has constructed an improved and more relaxed protein–ligand complex, which can be analyzed for further studies. The increase in the RMSD value at the beginning of the simulation shows that AC5 adopts a much more extended conformation.

Comparison between the Ramachandran plots of protein before and after MD cleared that there are some differences in the backbone of dihedral angle values which slightly affect the position of some residues in the Ramachandran plots. As it can be seen in Fig. 7a, b, the presence of the ligand in the active site of protein during MD simulation leads to the displacement of these residues into the disallowed regions. In other words, before the beginning of MD, the protein has no residues in the generously allowed or disallowed regions of the Ramachandran plot, but after the MD, 1.6 % of the residues move to these unsuitable regions.

The RMSD of the ligand was calculated based on the MD simulation of the system to obtain information on position fluctuations and movements of ligand's atoms. Figure 8 showed that the RMSD of the ethyl betulinic acid increased from the initial conformation to 0.1 Å after 2.5 ns and dropped suddenly to 0.4 Å. After fluctuating at about 3 ns, it rose up again to about 0.8 Å. This indicated that, after 8 ns simulation and preliminary fluctuations in the magnitude of RMSD of ligand's atoms, the ligand obtained an equilibrium state characterized by the RMSD profile.

At the end of MD, position and orientation of ligand in the introduced binding site were changed, and this important observation indicates useful application of MD after

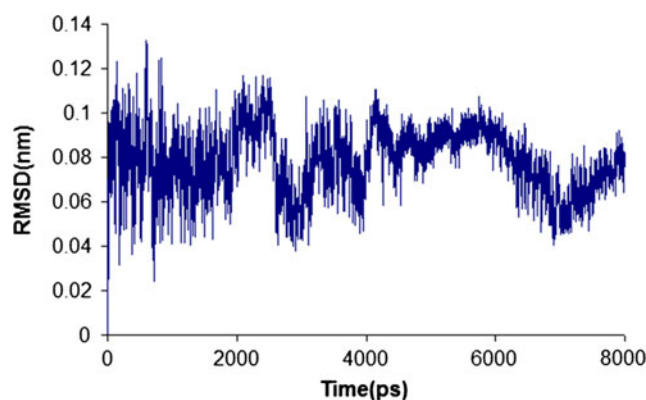


Fig. 8 RMSD of ethyl betulinic acid during the 8 ns molecular dynamic simulation

docking of ligands in the binding pocket. Explorative run of MD on the complex between the protein and the investigated ligand revealed that almost all residues of the active site determined by docking were changed and some new residues such as Arg197, Glu198, and Asp199 are positioned in proximity of ligands and could participate in the interaction (Fig. 9).

Arg140 assembles one hydrophilic interaction with ligand, which accommodates the hydroxyl moiety of the ligand in position 3. Hence, if we change hydroxyl group of this position with hydrophobic groups, this interaction is vanished and reduction of effect is observed. Alternatively, in position 28, which has two major interactions including hydrophobic interaction with Val195 and Met194 and hydrophilic interaction with Asn200 and Asp199 (Fig. 10), substitution with a group with both hydrophilic and hydrophobic characteristics, such as ethyl acetate, the maximum of interactions will occur. Accordingly, phagocytic oxidative burst activity by betulinic acid (**2**) with the acidic hydrophilic group on C-28 or lupeol

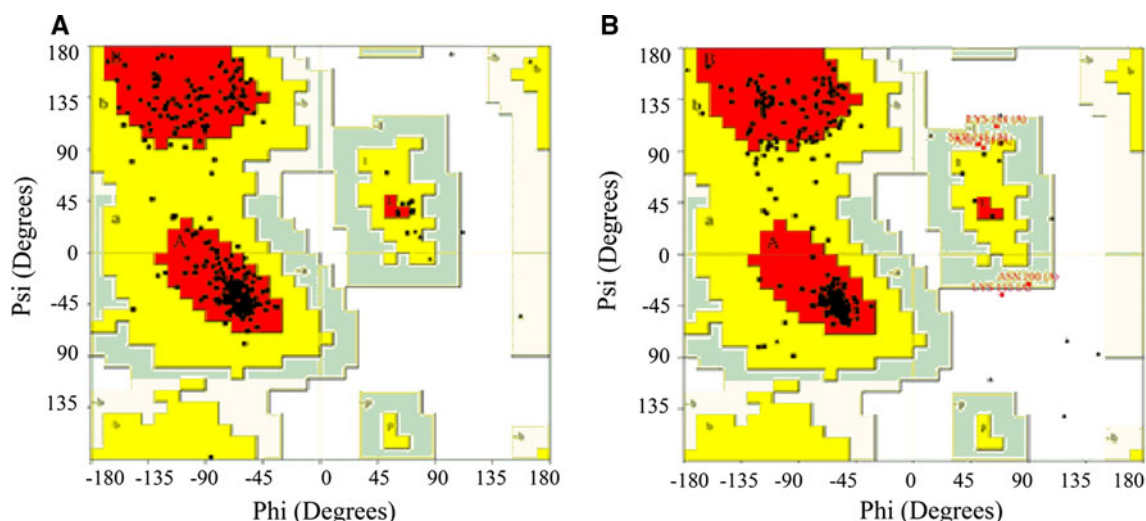


Fig. 7 Ramachandran plot of adenylyl cyclase type 5 protein; **a** before and, **b** after molecular dynamic simulation

Fig. 9 3D representation of ethyl betulinate in the binding site of adenylyl cyclase 5 after molecular dynamic simulation

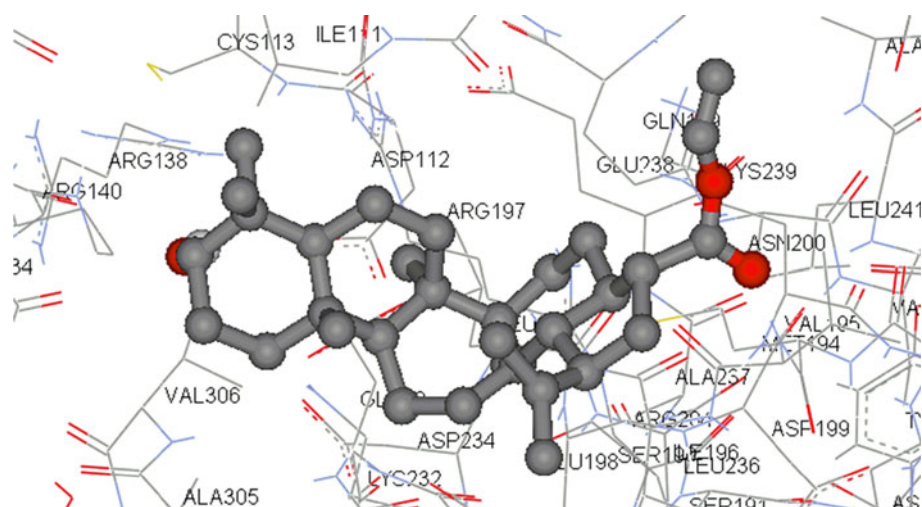
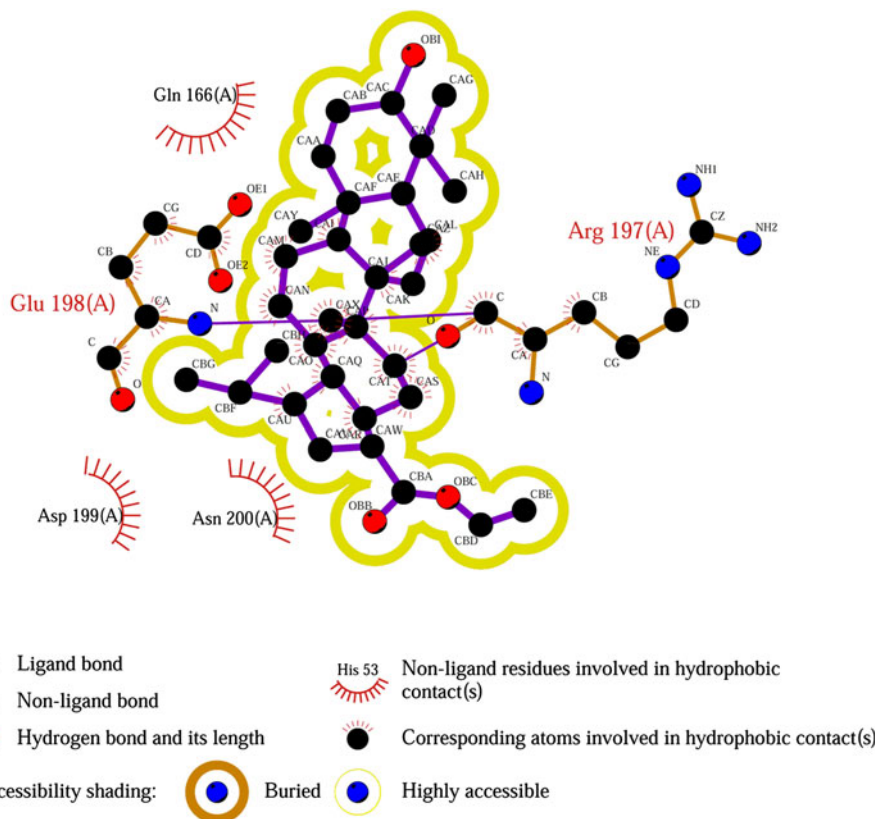


Fig. 10 2D representation of interactions between ethyl betulinate and adenylyl cyclase 5



with the methyl hydrophobic group are weaker than ethyl betulinate (**3**) with the amphoteric esteric group on C-28 (Fig. 1). It was in agreement with other reports on C-28 amide derivatives of betulinic acid reported as more potent inhibitors of tumor cell growth (Shintyapina *et al.*, 2007). To date, there exist other reports also in the literature describing the chemical modification of lupane-type triterpenes to produce derivatives with enhanced anti-HIV and cytotoxic activities (Baglin, 2003), but little is known about the importance of the various functional groups in this skeleton for the expression of

immunomodulatory properties, especially on C-28; Therefore, testing other derivatives by modification on this position is suggested to improve their immunosuppressant effects.

Conclusion

By means of a computational approach, integrating molecular docking and molecular dynamics simulation of lupol derivatives on adenylyl cyclase 5 provided strong

evidence for these compounds as potential activators of AC. These results are consistent with other studies on the activation of AC and increasing cAMP level as possible routes for the reduction of neutrophil oxidative burst or regulation of T cell proliferation (Bani *et al.*, 2006; Yeadon and Diamant, 2000).

Acknowledgments The authors are grateful to prof. Dr. Muhammad Iqbal Choudhary, and the H. E. J. Research Institute of Chemistry, International Center for Chemical and Biological Sciences, University of Karachi, for their financial supports.

References

- Aandahl EM, Moretto WJ, Haslett PA, Vang T, Bryn T, Tasken K, Nixon DF (2002) Inhibition of antigen-specific T cell proliferation and cytokine production by protein kinase A type I. *J Immunol* 169:802–808
- Ayatollahi AM, Ghanadian M, Afsharypour S, Abdalla OM, Mirzai M, Askari G (2011) Pentacyclic triterpenes in *Euphorbia microsciadia* with their t-cell proliferation activity. *Iran J Pharm Res* 10:287–294
- Baglin I, Mitaine-Offer AC, Nour M, Tan K, Cave C, Lacaille-Dubois MA (2003) A review of natural and modified betulinic acid, ursolic and echinocystic acid derivatives as potential antitumor and anti-HIV agents. *Mini Rev Med Chem* 3:525–539
- Bani S, Kaul A, Khan B, Ahmad SF, Suri KA, Gupta BD, Satti NK, Qazi GN (2006) Suppression of T lymphocyte activity by lupeol isolated from *Crataeva religiosa*. *Phytother Res* 20:276–287
- Berendsen H, Postma J, van Gusteren W, Hermans J (1981) Interaction models for water in relation to protein hydration. Reidel, Dordrecht
- Darden T, York D, Pedersen L (1993) Particle mesh Ewald: an N-log(N) method for Ewald sums in large systems. *J Chem Phys* 98:10089–10092
- Domínguez-Carmona DB, Escalante-Erosa F, García-Sosa K, Ruiz-Pinell G, Gutierrez-Yapu D, Chan-Bacab MJ, Giménez-Turba A, Pena-Rodríguez LM (2010) Antiprotozoal activity of betulinic acid derivatives. *Phytomedicine* 17:379–382
- Einzhammer DA, Xu ZQ (2004) Betulinic acid: a promising anticancer candidate. *Idrugs* 4:359–373
- Erickson JA, Jalaie M, Robertson DH, Lewis RA, Vieth M (2004) Lessons in molecular recognition: the effects of ligand and protein flexibility on molecular docking accuracy. *J Med Chem* 47:45–55
- Gasteiger J, Marsili M (1980) Iterative partial equalization of orbital electro- negativity—a rapid access to atomic charges. *Tetrahedron* 36:3219–3228
- Helen L, Robert J, Roger C, Steven W (2010) Neutrophil function in inflammation and inflammatory diseases. *Rheumatology* 49:1618–1631
- Hess B, Bekker H, Berendsen H, Fraahje J (1997) LINCOS: a linear constraint solver for molecular interactions. *J Comp Chem* 18:1463–1472
- Humphrey W, Dalke A, Schulten K (1996) VMD: Visual molecular dynamics. *J Mol Graph* 14:33–38
- Lobstein A, Schoonjans K, Souchet M, Auwerx J, Saladin R, Wagner A (2010) Structure-activity relationship study of betulinic acid, a novel and selective TGR5 agonist, and its synthetic derivatives: potential impact in diabetes. *J Med Chem* 53:178–190
- Macias FA, Simonet AM, Esteban DM (1994) Potential allelopathic lupane triterpenes from bioactive fractions of *Melilotus messanensis*. *Phytochemistry* 36:1369–1379
- Mischak H, Goodnight JA, Kolch W, Martiny-Baron G, Schaechtle C, Kazanietz MG, Blumberg PM, Pierce JH, Mushinski JF (1993) Overexpression of protein kinase C-delta and epsilon in NIH 3T3 cells induces opposite effects on growth, morphology, anchorage dependence, and tumorigenicity. *J Biol Chem* 268:6090–6096
- Morris GM, Goodsell DS, Halliday RS, Huey R, Hart WE, Belew RK, Olson AJ (1998) Automated docking using a Lamarckian genetic algorithm and an empirical binding free energy function. *J Comput Chem* 19:1639–1662
- Nielsen MB, Gerwien J, Nielsen M, Geisler C, Ropke C, Svejgaard A (1998) MHC class II ligation induces CD58 (LFA-3)-mediated adhesion in human T cells. *Exp Clin Immunogenet* 15:61–68
- Ottonello L, Morone MP, Dapino P, Dallegri F (1995) Cyclic AMP-elevating agents down-regulate the oxidative burst induced by granulocyte-macrophage colony-stimulating factor (GM-CSF) in adherent neutrophils. *Clin Exp Immunol* 101:502–506
- Ruppelt A, Mosenden R, Grönholm M, Aandahl EM, Tobin D, Carlson CR, Abrahamsen H, Herberg FW, Carpén O, Taskén K (2007) Inhibition of T cell activation by cyclic adenosine 5'-monophosphate requires lipid raft targeting of protein kinase A type I by the A-kinase anchoring protein ezrin. *J Immunol* 179:5159–5168
- Shahlaei M, Madadkar-Sobhani A, Fassihi A, Saghale L (2011a) Exploring a model of a chemokine receptor/ligand complex in an explicit membrane environment by molecular dynamics simulation: the human CCR1 receptor. *J Chem Inf Model* 51:2717–2730
- Shahlaei M, Madadkar-Sobhani A, Mahnam K, Fassihi A, Saghale L, Mansourian M (2011b) Homology modeling of human CCR5 and analysis of its binding properties through molecular docking and molecular dynamics simulation. *Biochim Biophys Acta Biomembr* 1808:802–817
- Shintyapina AB, Shults EE, Petrenko NI, Uzenkova NV, Tolstikov CA, Pronkina NV, Kozhevnikov VS, Pokrovsky AG (2007) Effect of nitrogen-containing derivatives of the plant triterpenes betulin and glycyrrhetic acid on the growth of MT-4, MOLT-4, CEM, and Hep G2 tumor cells. *Russ. J Bioorg Chem* 33:579–583
- Solis FJ, Wets JB (1981) Minimization by random search techniques. *Math Oper Res* 6:19–30
- Viqar UA, Rahman AU (1994) Handbook of natural products data, vol 2. Elsevier Sciences, Amsterdam
- Weiner SJ, Kollman PA, Case DA, Singh UC, Ghio C, Alagona G, Profeta S, Weiner PK (1984) A new force-field for molecular mechanical simulation of nucleic-acids and proteins. *J Am Chem Soc* 6:765–784
- Yeadon M, Diamant Z (2000) New and exploratory therapeutic agents for asthma. Marcel Dekker, New York
- Yi JE, Obminska-Mrukowicz B, Yuan LY, Yuan H (2010) Immunomodulatory effects of betulinic acid from the bark of white birch on mice. *J Vet Sci* 11:305–313
- Yogeeswari P, Sriram D (2005) Betulinic acid and its derivatives: a review on their biological properties. *Curr Med Chem* 12: 657–666